

Functional Fatigue and Tension–Compression Asymmetry in [001]-Oriented $\text{Co}_{49}\text{Ni}_{21}\text{Ga}_{30}$ High-Temperature Shape Memory Alloy Single Crystals

P. Krooß^{1,8} · T. Niendorf^{1,8} · P. M. Kadletz² · C. Somsen³ · M. J. Gutmann⁴ · Y. I. Chumlyakov⁵ · W. W. Schmahl² · G. Eggeler³ · H. J. Maier^{6,7}

Published online: 21 April 2015
© ASM International 2015

Abstract Conventional shape memory alloys cannot be employed for applications in the elevated temperature regime due to rapid functional degradation. Co–Ni–Ga has shown the potential to be used up to temperatures of about 400 °C due to a fully reversible superelastic stress–strain response. However, available results only highlight the superelastic response for single cycle tests. So far, no data addressing cyclic loading and functional fatigue are available. In order to close this gap, the current study reports on the cyclic degradation behavior and tension–compression asymmetry in [001]-oriented $\text{Co}_{49}\text{Ni}_{21}\text{Ga}_{30}$ single crystals at elevated temperatures. The cyclic stress–strain response of the material under displacement

controlled superelastic loading conditions was found to be dictated by the number of active martensite variants and different resulting stabilization effects. Co–Ni–Ga shows a large superelastic temperature window of about 400 °C under tension and compression, but a linear Clausius–Clapeyron relationship could only be observed up to a temperature of 200 °C. In the present experiments, the samples were subjected to 1000 cycles at different temperatures. Degradation mechanisms were characterized by neutron diffraction and transmission electron microscopy. The results in this study confirm the potential of these alloys for damping applications at elevated temperatures.

Keywords Shape memory alloy (SMA) · Martensitic phase transformation · Internal friction · Martensite stabilization · Superelasticity

✉ H. J. Maier
maier@iw.uni-hannover.de

¹ Lehrstuhl für Werkstoffkunde (Materials Science), University of Paderborn, 33098 Paderborn, Germany

² Applied Crystallography, Department of Earth and Environmental Sciences, Ludwig-Maximilians-Universität, 80333 Munich, Germany

³ Institut für Werkstoffe, Ruhr-Universität Bochum, 44801 Bochum, Germany

⁴ ISIS Facility, Rutherford Appleton Laboratory, Chilton, Didcot, Oxfordshire OX11 0QX, UK

⁵ Siberian Physical Technical Institute, Tomsk State University, Novosobornay Square 1, 634050 Tomsk, Russia

⁶ Institut für Werkstoffkunde (Materials Science), Leibniz Universität Hannover, 30823 Garbsen, Germany

⁷ Zentrum für Festkörperchemie und Neue Materialien, Leibniz Universität Hannover, 30167 Hannover, Germany

⁸ Present Address: Institut für Werkstofftechnik, Technische Universität Bergakademie Freiberg, 09599 Freiberg, Germany

Introduction

Shape memory alloys (SMAs) have been studied intensely for decades owing to their complex nature of thermo-mechanical deformation governing their unique properties [1–3]. As a result of a reversible transformation between a high-temperature austenitic parent phase and a low-temperature martensitic product phase, conventional SMAs can accomplish maximum transformation strains of the order of 10 % [1–3]. Based on the transformation temperatures for the martensitic and the austenitic transformation (M_s , M_f , A_s , A_f), different types of effects can be observed [1, 3]. The one-way shape memory effect, the two-way shape memory effect and superelasticity (SE) are the three basic mechanisms solely observed in shape memory materials [1, 3].

Given the large specific work output of these materials, highly efficient solid-state actuators and damping devices

with extremely low weight can be realized [1–3]. As they also work silently, a broad range of applications for SMAs can be envisaged. Still, SMAs are only used in niche applications such as stents or surgical devices in the biomedical sector [1, 3, 4]. Several drawbacks hinder the widespread use of SMAs. For example, Ni–Ti alloys suffer from high production costs. SMAs that contain only cheaper elements and can be processed by traditional metallurgical routes, e.g., the Fe-based alloys proposed in the last decades, mostly suffer from low transformation strains or microstructural instability under cyclic loading [1, 3, 5–7]. Thus, the functional and structural fatigue are, amongst others, key issues that need to be addressed in the development of novel SMAs [1–4].

Another roadblock that limits widespread application of SMAs is their low maximum operating temperature. Conventional SMAs such as Ni–Ti can only be employed in actuation applications up to temperatures of about 100 °C [2]. For Ni–Ti, these limitations arise primarily from the low martensite start temperature. Numerous other alloys, e.g., Cu-based SMAs, suffer aging-induced changes in transformation temperatures imposed by martensite stabilization [8–11]. Many devices working at elevated temperatures would benefit from solid-state actuators and dampers. Therefore, tremendous effort has been spent in the development of suitable alloys that feature elevated M_s and at the same time withstand functional degradation [1, 2, 8–16].

High-temperature shape memory alloys (HT-SMAs) have been mainly developed for applications in aerospace, automotive, energy exploration, and conversion industries, where the operating temperatures are often well above 100 °C [2]. Particularly HT-SMAs such as Ni–Ti–X ($X = \text{Pt, Pd, Au, Hf, Zr}$) and Zr–Cu-based alloys have been studied in detail lately [2, 17–20]. However, either their poor workability or the extremely high cost of the constituent elements typically hinder widespread applications of these alloys.

For actuation at elevated temperatures the Ti–Ta system has been proposed as a promising alternative [15, 16]. The material can be cold worked to high degrees of deformation reducing manufacturing costs significantly. However, pseudoelasticity (PE) has not been demonstrated for Ti–Ta HT-SMAs. In addition, rapid functional degradation represents another issue hindering application so far [15, 16]. Ternary elements hamper degradation, but cannot fully stabilize the microstructure at elevated temperatures [16]. For a more comprehensive review on HT-SMAs the reader is referred to a recent paper by Ma et al. [2].

Co–Ni–Ga is a potential HT-SMA as it shows high transformation strains in a large temperature window. The maximum temperature for PE has been reported to be about 400 °C [21]. At the same time formability of the alloy can be adjusted by incorporation of the disordered secondary

γ -phase (A1) [2, 21–23]. Generally, Co–Ni–Ga alloys undergo a martensitic transformation to a tetragonal structure ($L1_0$) from the high-temperature cubic B2-structured austenite [12, 14, 21–26]. Co–Ni–Ga HT-SMAs have been characterized intensely in recent years. Structural and phase transformation characteristics as well as the general superelastic behavior up to temperatures of about 400 °C [12, 14, 21–29] have been thoroughly examined.

The main focus of these studies was on transformation strains, transformation stresses, and thermal hysteresis within single cycle tests or within incremental strain tests [29], as a function of temperature under tensile or compressive loading. However, in many of the envisaged applications, the Co–Ni–Ga HT-SMAs will undergo both tensile and compressive deformation in a cyclic fashion for a high number of cycles. Thus, it is mandatory to characterize the cyclic superelastic behavior with respect to the stress state and identify the microstructural mechanisms responsible for cyclic degradation.

The objective of the present study was to shed light on the cyclic superelastic behavior of [001]-oriented $\text{Co}_{49}\text{Ni}_{21}\text{Ga}_{30}$ crystals in tension and compression. The [001]-orientation was selected to minimize dislocation slip in the B2-ordered alloy due to an extremely low Schmid factor [30]. Cyclic superelastic testing up to the maximum transformation strains, i.e., 4.6 % in compression and 7.5 % in tension, was conducted up to 1000 cycles in the temperature range from 100 to 400 °C. Analyses of microstructural evolution allowed for solid conclusions regarding the mechanisms that contribute to functional degradation in Co–Ni–Ga HT-SMAs.

Materials and Experimental Techniques

Ingots of Co–Ni–Ga with a nominal composition of 49Co–21Ni–30Ga (in at.%) were produced using vacuum induction melting. The present composition was chosen as the A_f temperature of the $\text{Co}_{49}\text{Ni}_{21}\text{Ga}_{30}$ alloy is slightly below room temperature [21], leading to a PE response in the whole range of test temperatures employed. Large single crystals were grown using the Bridgman technique in a He environment. For compression tests, specimens with dimensions of $4 \times 4 \times 8$ mm were electro-discharge machined from the bulk single crystals such that their longer loading axes were oriented along the [001] direction in austenite. For tensile testing dog-bone-shaped samples with a gage length of 6 mm and a cross section of 1.5×1.5 mm were machined from the bulk material along the [001] austenite orientation. Samples were tested in the as-grown condition for ease of comparison with data available in literature, e.g., [21, 22, 29].

In order to characterize the initial response of the alloy, quasi-static uniaxial single cycle tests in compression and

tension at constant temperature levels ranging from 50 to 400 °C were performed using an MTS servo-hydraulic test frame in displacement control mode with a fixed maximum strain upon loading and a given minimum stress for unloading. Given the significant difference in stress–strain response under tension and compression, the crosshead displacement rates were adjusted to yield identical cycle times for each stress state. This resulted in nominal strain rates of 5×10^{-4} and $3 \times 10^{-4} \text{ s}^{-1}$ in tension and compression, respectively. Strains were measured using a high-temperature extensometer with a gage length of 12 mm attached to the grips in case of compression testing. For calculation of the nominal strain in these tests the grips were treated as absolutely rigid. In case of the tensile experiments the transformation strains were much higher than those theoretically predicted by Dadda et al. and Monroe et al., i.e., 4.3 and 8.5 % in compression and tension, respectively [26, 29]. Strains in the tensile tests were also calculated from displacement data, and a reference test at RT employing a miniature extensometer featuring a gage length of 3 mm was employed for calibration purpose. Heating of all samples was performed by convective heating. Temperatures were measured with a thermocouple attached to the sample surface by a steel spring.

Superelastic cycling experiments under tension and compression were performed at temperatures ranging from 100 to 300 °C for up to 1000 cycles in order to investigate the functional stability. The maximum strain levels for the fatigue tests were set to 4.6 % in compression and 7.5 % in tension, respectively, corresponding to the theoretical maximum values according to literature.

Neutron diffraction experiments were conducted for as-grown and fatigued tensile samples using the single crystal diffractometer SXD [31] at the ISIS neutron source, Rutherford Appleton Laboratory, Oxfordshire. Neutron diffraction is favorable when sample volumes with dimensions of mm^3 to cm^3 have to be probed because the attenuation length of neutrons is typically in the order of cm to m and therefore, relatively large as compared to the attenuation length of X-rays or electrons. SXD uses the time-of-flight (TOF) Laue technique employing a white beam with incident wavelengths covering a range of 0.2–10 Å. Eleven ZnS-type scintillator detectors are arranged around the sample position covering a large volume in reciprocal space. This allows scanning large 3D volumes and collecting complete diffraction patterns within a relatively short time with only three to five sample orientations. Data were indexed and integrated using the software package SXD2001. Peak widths for (110) and (350) were extracted using only reflections from the backscattering detectors which yield the best resolution in $\Delta d/d$, where d is the lattice spacing.

Microstructural analyses were conducted using a FEI Tecnai F20 operating at 200 kV equipped with a Gatan

double-tilt high-temperature stage in order to correlate microstructural features with the observed thermo-mechanical behavior. The TEM samples were first mechanically ground and polished down to a thickness of 0.15 mm. Finally, electron transparent areas were obtained using twin-jet polishing with a solution of 600 ml methanol, 340 ml butanol, and 60 ml perchloric acid under an applied potential of 70 V at a temperature of -25 °C .

Results

Cyclic Stress–Strain Response

Figures 1 and 2 show the results from the superelastic cycling experiments revealing the transformation behavior of the as-grown $\text{Co}_{49}\text{Ni}_{21}\text{Ga}_{30}$ shape memory alloy in the temperature range between 100 and 300 °C under compressive and tensile loading. From the stress–strain curves shown in Fig. 1, it is apparent that [001]-oriented Co–Ni–Ga single crystals show perfect cyclic stability at 100 °C during 1000 superelastic compression cycles with a maximum strain of 4.6 %, i.e., close to the maximum theoretical value of exploitable reversible strain for Co–Ni–Ga under compressive load at RT [29]. When interpreting the data of the current study, one needs to take into account that the maximum absolute strain value was always used as the strain limit for testing. Thus, superelastic strain, i.e., the portion of strain linked to the stress plateau stemming from phase transformation, changed due to the increase in the critical stress for stress-induced martensite transformation (σ_{crit} for SIMT) and concomitantly the portion of elastic strain of austenite with increasing test temperature, cf. Fig. 1. At 100 °C, the Co–Ni–Ga specimen is characterized by a σ_{crit} of about 190 MPa throughout the whole test. An increase in test temperature to 200 °C results in an increase of σ_{crit} to a value of about 400 MPa in the 1st cycle. In the following cycles at 200 °C a decrease of σ_{crit} is seen, indicating cyclic instability. In the 1000th cycle σ_{crit} decreased to about 250 MPa. Furthermore, about 0.3 % of

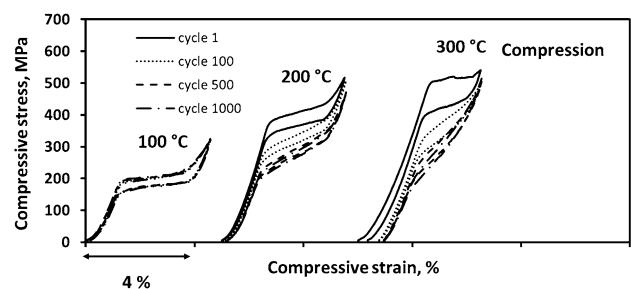


Fig. 1 Cyclic stress–strain response of [001]-oriented Co–Ni–Ga single crystals under compression

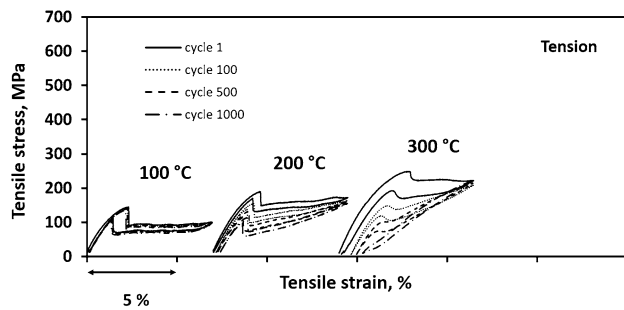


Fig. 2 Cyclic stress–strain response of [001]-oriented Co–Ni–Ga single crystals under tension

permanent strain accumulated after 1000 cycles. At 300 °C, cyclic degradation becomes even more rapid and σ_{crit} decreases from about 480 to 350 MPa before 100 cycles is reached.

Figure 2a shows a similar behavior under tensile loads, despite the fact that for a given temperature transformation stresses are significantly lower than in compression testing. Figure 2 demonstrates that the material shows perfect cyclic stability during superelastic cycling at 100 °C. Maximum total strains of 7.5 % were employed in this test as this value is close to the theoretical maximum of transformation strain under tension in the Co–Ni–Ga system [26]. Although the maximum strain value employed in the tensile tests was significantly larger than the one used under compression, the stress–strain response remained stable during 1000 cycles. An increase in test temperature from 100 to 200 °C led to an increase in the initial σ_{crit} for SIMT from about 150 MPa to about 200 MPa. With increasing number of superelastic cycles a substantial decrease in σ_{crit} occurred at 200 °C (cf. Fig. 2). This observation is in good agreement with the results obtained under compression (Fig. 1) and further emphasizes the strong impact of test temperature on the cyclic deformation behavior of Co–Ni–Ga HT-SMAs. An increase of the test temperature to 300 °C resulted in a rapid accumulation of residual strain and a pronounced change in the stress–strain response. Similar to the compression case, an almost full degradation of the Co–Ni–Ga sample is seen after 1000 cycles at 300 °C (Fig. 2).

As temperature affects the cyclic stress–strain response under both, compressive and tensile loads in [001]-oriented Co–Ni–Ga HT-SMA specimens similarly, it seems reasonable to assume that the microstructural mechanisms leading to functional degradation are similar in both cases. Both the steady decrease of σ_{crit} for SIMT as well as the evolution of permanent strain following PE cycling are qualitatively similar for tension and compression tests at temperatures above 200 °C.

In order to evaluate the current findings in more depth, the evolution of distinct values closely related to the SIM

are elaborated in more detail—Figs. 3, 4, and 5. As detailed before, maximum strains for tensile and compressive tests were different in order to meet the targeted maximum theoretical values. This ensured that the largest fraction of the Co–Ni–Ga sample transformed in each case. For better comparability normalized permanent strains (nps) at test temperatures of 100, 200, and 300 °C are plotted in Fig. 3 for tension and compression during 1000 superelastic cycles. Up to 200 °C (stage 1) the evolution of accumulated permanent strain is found to be similarly small in tension and compression, and the nps remains below 0.08. An increase in test temperature to values above 200 °C (stage 2) leads to a generally accelerated permanent strain accumulation for both stress states, i.e., tension and compression. From Fig. 3, normalized permanent strain accumulation is more pronounced in compression. However, it should be noted that transformation strains are significantly different for both tension and compression as well. Thus, an nps of 0.3 in tension indicates a fully degraded condition, which also fits the neutron diffraction data (cf. “Neutron Diffraction and Electron Microscopy” section) that revealed 94 % remnant martensite. By contrast, in compression nps reaches values above 0.5 before the sample is fully degraded.

Figure 4 shows the Clausius–Clapeyron (CC) curves illustrating the asymmetric stress dependence of M_s and A_s for tensile and compressive loading. The CC slope for the transformation temperatures shown is higher for compressive loading. This results in higher stresses for forward and reverse transformations in compression than in tension at elevated temperatures, cf. Figs. 1 and 2. The slopes of the CC curves for the A_s temperature in tension and compression were found to be clearly different within the two previously defined temperature regimes, i.e., significantly lower in stage 2 ($T > 225$ °C).

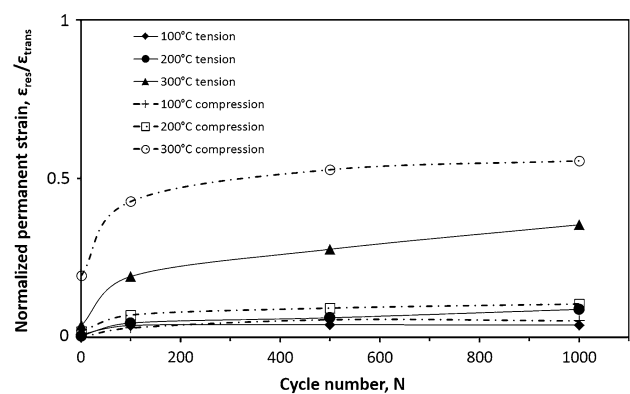


Fig. 3 Normalized permanent strain evolution up to 1000 superelastic cycles obtained from the fatigue experiments under tension and compression. The *dotted lines* show the results under compressive loads

Fig. 4 Clausius–Clapeyron relationship obtained from single cycle tests under tension and compression for M_s and A_s . Stage 1 refers to the low-temperature regime below 200 °C and stage 2 refers to the high temperature regime above 225 °C. The transition area is highlighted by gray color

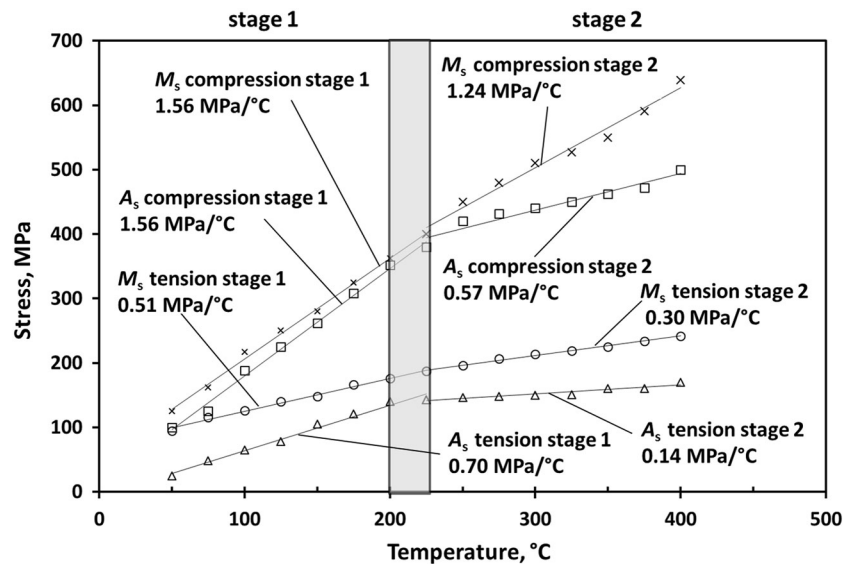
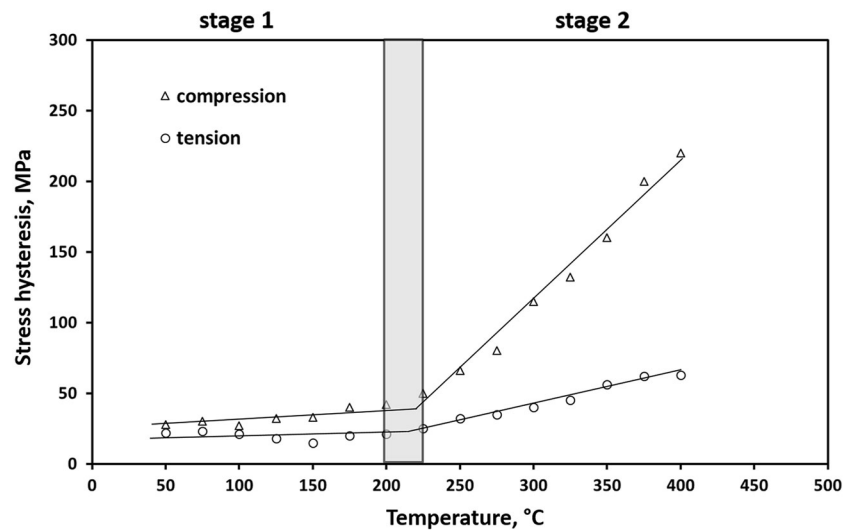


Fig. 5 Evolution of stress hysteresis width obtained from single cycle tests under tension and compression. Triangles represent the results under compressive loads. Stress hysteresis was determined based on the difference between the stress plateau upon loading and the stress plateau upon unloading at $\epsilon_{trans}/2$. Stage 1 refers to the low-temperature regime below 200 °C and stage 2 refers to the high-temperature regime above 225 °C. The transition area is highlighted by gray color



The evolution of the width of the stress hysteresis obtained from single cycle tests is shown in Fig. 5. Below 200 °C, the evolution of the stress hysteresis width is very similar under tension and compression. Above 225 °C the hysteresis width under compression increases more rapidly than under tension (Fig. 5). As can be deduced from Fig. 4, this tremendous change mainly stems from the non-linear evolution of A_s .

Neutron Diffraction and Electron Microscopy

Neutron diffraction was performed on a $\text{Co}_{49}\text{Ni}_{21}\text{Ga}_{30}$ single crystal tensile test sample in its initial as-grown state and on a reference tensile test sample that had been subjected to 1000 fatigue cycles at 300 °C. In the as-grown state the presence of a purely austenitic cubic structure was

confirmed, with a lattice parameter $a_0 = 2.867(2)$ Å. Weak superstructure reflections indicate B2-type ordering (space group $\text{Pm}\bar{3}\text{m}$). After fatigue the sample was composed of two component crystals of different phase state. Component one was indexed as body-centered tetragonal (bct) martensite with space group $\text{I4}/\text{mmm}$ and lattice parameters $a_{\text{bct}} = 2.732(1)$ Å and $c_{\text{bct}} = 3.179(2)$ Å. Component two was indexed as an axially strained austenite with lattice spacings of $d_{100/010} = 2.860(2)$ Å and $d_{001} = 2.921(2)$ Å. The comparison of diffraction intensities of the two detected phases allows a quantitative determination of the volume ratios: 94 ± 2 % martensite and 6 ± 2 % axially strained austenite. The martensitic bct structure can also be referred to as face-centered tetragonal (fct) L1_0 -type structure using the lattice relations $a_{\text{bct}} \cdot \sqrt{2} = a_{\text{L10}}$ and $c_{\text{bct}} = c_{\text{L10}}$ resulting in $a_{\text{L10}} = 3.863(3)$ Å and

$c_{L10} = 3.179(2)$ Å for the fct unit cell. The elongated axes of component one (martensite) and component two (axially strained austenite) are oriented parallel to the sample load axis and represent the sample state in the load-free condition after fatigue. Peak widths were extracted from the data using peaks only on detectors in backscattering direction where the $\Delta d/d$ resolution is optimal. For determination of peak widths, several reflections of symmetrically equivalent lattice planes on equivalent spots of the area detectors were taken and the average peak width was calculated in TOF as well as horizontal and vertical (x - and z -) detector direction (Figs. 6, 7). The TOF value of certain reflections represents the d -spacing of corresponding lattice planes; peak widths in x - and z -detector directions are related to orientational variations of the diffracting crystal and thus they reflect mosaicity of the single crystal and component single crystal, respectively. Correspondingly, the x - and z -broadening of the reflections was converted to mosaicity in units of degrees. Z -coordinates are oriented parallel and x -coordinates are oriented perpendicular to the loading axis of the fatigue experiments (a detailed description of the SXD coordinate system can be found in [31]). A representation of 110 and 350 reflections is shown in Fig. 6. Reflections from the {110} and {350} lattice planes of (i) austenite in its initial state from the as-grown sample and (ii) axially strained austenite as well as martensite from the fatigued sample showed a number of peaks on the backscattering detectors allowing direct comparison.

In order to further correlate the current findings to microstructure evolution, TEM investigations were carried out. Based on the results from the fatigue experiments (cf. Fig. 3), qualitatively similar mechanisms are assumed to govern cyclic degradation for both, tensile and compressive loads. As dislocation activity and dislocation-phase

boundary interactions were main aspects of the TEM investigation, tensile samples with a low absolute value of σ_{crit} for SIMT were chosen to minimize dislocation slip. Figure 8 shows TEM micrographs of a tension sample after 1000 superelastic cycles at 300 °C. The reflection spots recorded from the area marked by the white circle in Fig. 8b reveal a fully stabilized martensitic microstructure (Fig. 8c). The black arrows in Fig. 8a show the presence of a few dislocations, mainly in the vicinity of small additional martensite variants, which appear bright due to the imaging conditions selected. Intense dislocation activity at interfaces under tensile loading has been further substantiated by additional TEM analyses including weak-beam imaging (not shown for the sake of brevity). From the differences in stress hysteresis between compression and tension, one could expect a higher dislocation density for the compression case. This could explain the very rapid increase in the nps value in the compression for the 300 °C case. However, for the evolution of degradation the local dislocation density at the interfaces is important. In fact, Fig. 8a demonstrates that despite a low average dislocation density in the matrix, this can be sufficient to stabilize the martensite by concentration of the dislocations at interfaces. Clearly, quantitative analysis of local dislocation density evolution upon cyclic deformation in tension and compression is challenging and needs to be addressed in future work. When this sample was heated to 500 °C in situ in the TEM it remained in its stabilized martensitic condition. This stabilization phenomenon provides a good explanation for the observed cyclic degradation of the 300 °C sample and underlines the findings of the neutron experiments. After 1000 cycles at 300 °C, which implies a total time of 8.5 h at 300 °C, no precipitates were detected in the stabilized martensitic matrix.

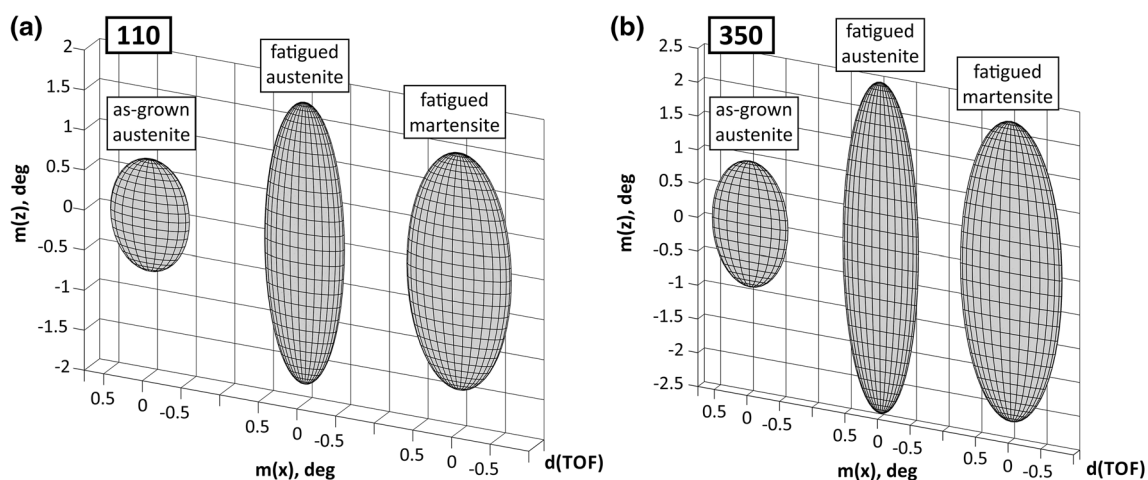


Fig. 6 Three-dimensional **a** 110 and **b** 350 peak profiles of as-grown austenite and fatigued austenite and fatigued martensite. A slight z -axis broadening of the as-grown state is due to the elongated sample

geometry being mapped onto the detector. Mosaicity in horizontal (x -) and vertical (z -) detector direction, $m(x)$ and $m(z)$, is given in degrees

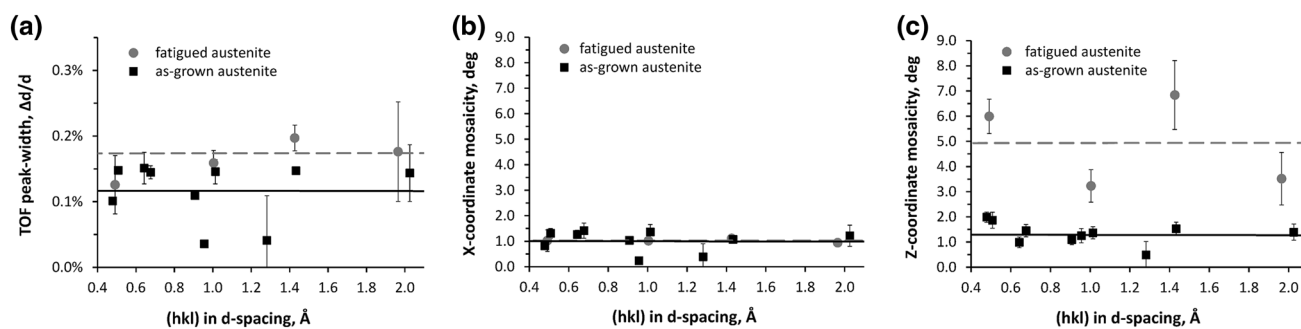
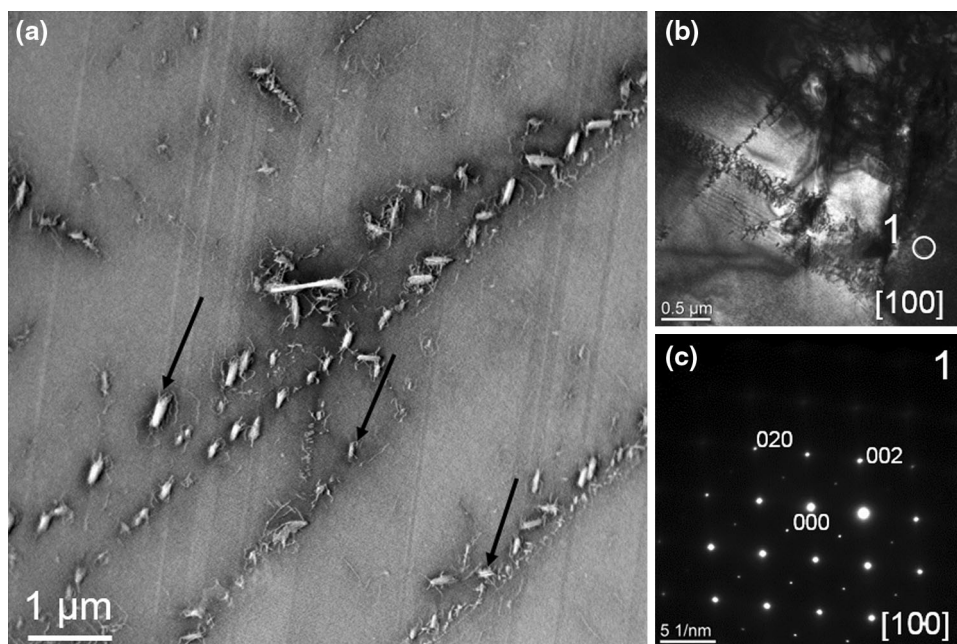


Fig. 7 Peak widths in **a** TOF direction and mosaicity in **b** *x*- and **c** *z*-coordinate direction plotted over the *d*-spacing of their corresponding reflections. TOF peak widths are given in $\Delta d/d$, mosaicity is given in degrees and *d*-spacings are given in Ångström

Fig. 8 TEM results from a sample fatigued at 300 °C for 1000 cycles in tension. **a** STEM overview. **b** Local region where SAED was taken. **c** SAED revealing the presence of martensite. For details see text



Discussion

The experimental observations indicate that the cyclic stress–strain response under compressive and tensile loads in Co–Ni–Ga HT-SMAs is affected by similar mechanisms that trigger functional degradation. Both decreasing stress values for the onset of the martensite transformation and a lower degree of reversibility of the phase transformation were found during superelastic cycling above 200 °C.

Figure 3 illustrates that the stress state, i.e., tensile and compressive stress, respectively, has only a small effect on the evolution of normalized permanent strain up to 200 °C. This is attributed to the high matrix hardness, which provides for an adequate resistance against dislocation plasticity [32]. Upon an increase in the test temperature a more pronounced defect generation sets in, as indicated by the evolution of the permanent strain for both stress states, Fig. 3. Especially the accumulation of permanent strain in

compression increases noticeably up to 0.43 nps at 300 °C, whereas it reached only 0.07 nps at 200 °C. At least three mechanisms are capable of stabilizing the martensitic phase: (i) the pinning of phase boundaries by boundary-dislocation interaction, (ii) diffusion-controlled precipitation, and (iii) diffusion-controlled ordering in the solid solution, associated with a change in symmetry conforming short-range ordering (SC-SRO) as proposed by Ren and Otsuka [7–11, 32].

The CC slopes shown in Fig. 4 demonstrate a significantly different temperature–stress relationship for the two stress states, resulting in significantly higher transformation stresses in compression than in tension. The results from the tensile tests in this study are in good agreement with those from Monroe et al. [26]. The authors reported a CC slope of about 0.7 MPa/ °C in the temperature range of 50–200 °C with respect to the evolution of the peak stress in stage 1. In the current work 0.51 MPa/ °C for M_s under

tension is found. The slight differences might be explained by the use of different single crystals with slightly different chemical composition. In stage 2 the slope for M_s decreased to about 0.3 MPa/°C. A more significant difference could be observed in compression experiments regarding the CC slope from Dadda et al. [21, 22] with 1.9 MPa/°C compared to 1.56 MPa/°C for M_s observed in this study. This again may be explained by the use of different single crystals. However, clear evidence cannot be provided at this point, as only nominal compositions are given in the aforementioned studies as well [21, 22]. In stage 2 the slope of M_s decreases to about 1.24 MPa/°C. However, general trends remain unaffected, i.e., the CC slope for Co–Ni–Ga tested in tension is significantly lower than for compression. In general, higher CC slopes should lead to a more intense dislocation activity as the temperature, at which the yield strength of the matrix is exceeded, becomes lower. Thus, for similar matrix hardness in compression and tension, compressive loads are supposed to result in a more intense dislocation activity at elevated temperatures. Considering the stress state it is obvious that the difference in normalized permanent strain in Fig. 3 between tension and compression at 300 °C can partly be related to the significantly higher stresses in compression (up to 500 MPa) as compared to tension (up to 200 MPa), Fig. 4. In recent studies the accumulation of permanent strain in SMAs was explained by the formation of retained martensite, mechanically stabilized by the stress fields of the dislocations formed during phase transformation [7, 32, 33]. These stress fields can stabilize evolving martensite variants as they form next to the phase boundaries, especially in case of repeated phase transformations during cyclic loading [7, 32, 33]. Consequently, the aforementioned conventional irreversible mechanisms would lead to a more intense cyclic degradation under compression.

Results from single cycle tests were analyzed in more depth for a detailed evaluation of the mechanisms that lead to the functional degradation, i.e., the accumulation of permanent strain in stage 2 above 200 °C. The CC Slopes for M_s and A_s temperatures are shown in Fig. 4 and the stress hysteresis widths are shown in Fig. 5. Figure 5 clearly indicates that in stage 2 the stress hysteresis under compression increases drastically while the stress hysteresis under tension only changes slightly. This indicates that above a critical temperature, energy dissipation due to frictional processes at the austenite–martensite interface and martensite variant boundaries plays a significant role [21, 22, 29, 34]. In addition to dislocation-controlled stabilization of the martensite phase other mechanisms may contribute to stabilization of the low-temperature phase [8–11]. Specifically, diffusion-controlled mechanisms such as precipitation of secondary phases or changes in SC-SRO need to be taken into account when discussing functional

degradation in Co–Ni–Ga alloys. Both mechanisms and their impact on the phase transformation behavior of SMAs have been studied extensively in the past [7–11, 21, 22, 29, 32, 34].

The CC slopes determined for A_s and M_s under tension and compression (Fig. 4) do help to understand which phase is stabilized by either a dislocation-controlled mechanism or changes in SC-SRO. The change in slope for A_s under tension and compression indicate a critical temperature of about 200–225 °C, above which the martensite phase is stabilized (Figs. 4, 5, stage 2). This is due to an increase in the required energy for reverse transformation. By contrast, the CC slope for M_s remains relatively constant with only a small decrease in stage 2. As a result, the stabilization of the martensitic phase leads to the pronounced increase of the width of the stress hysteresis above 200 °C (Fig. 5).

The changes in phase transformation behavior of Co–Ni–Ga single crystals during single cycle elevated temperature testing were already investigated by Dadda et al. [21, 22, 29, 34]. Using in situ techniques it was shown that above a critical temperature under compressive loads the phase transformation proceeds in a multi-variant martensite manner [22], while below 200 °C, the austenite–martensite transformation occurs with only one martensite variant being active. This also explains the small stress hysteresis and negligible accumulation of residual strain during cycling observed in the present study at lower temperatures (stage 1). For the high-temperature regime, i.e., stage 2, the interaction of multiple martensite variants is supposed to result in higher energy dissipation at the martensite variant boundaries [22]. This increase in internal frictional energy is macroscopically manifested in a larger stress hysteresis under compression as compared to tension (Fig. 5). At the same time tensile loads favor single martensite variants [23], which is in good agreement with the current results for the evolution of permanent strain as well as for stress hysteresis (Figs. 4, 5). Thus, the total number of martensite variants in Co–Ni–Ga HT-SMAs activated for a given stress state seems to govern both, the stress hysteresis width and the evolution of permanent strain (Fig. 3). However, this does not explain the qualitatively similar increase of normalized permanent strain with increasing number of cycles under both stress states (Fig. 3). Whereas both, the accelerated increase of the permanent strain in the very first cycles at 300 °C and the significant increase in stress hysteresis under compression in stage 2 result mainly from martensite variant interactions, diffusion-controlled mechanisms may play a key role for the subsequent increase of permanent strain with increasing number of cycles. The evolution of normalized permanent strain accumulated per cycle above 100 cycles (Fig. 3) is similar for both stress states. Given the significantly higher stresses

at 300 °C under compression and the higher dislocation activity at the martensite variant boundaries, diffusional processes appear to significantly affect the long-term cyclic behavior. It should be noted that the data shown in Figs. 4 and 5 were obtained from single cycle tests. As this implies a test time of about 30 s only, diffusional processes should be negligible and should therefore not contribute to stabilization of the martensite phase [14].

Chumlyakov et al. showed that small $L1_2$ γ' -precipitates form in Co–Ni–Ga at temperatures around 350 °C [35]. Niendorf et al. found that these precipitates even can nucleate at 300 °C during long-term aging in the austenite phase [36]. The aging time employed in [36] is equal to the test time in the fatigue tests in the current study. Thus, precipitation processes need to be taken into account for a better evaluation of the parameters affecting the superelastic cyclic deformation behavior. Various studies [24, 35, 36] revealed that a stabilization of the parent phase via the formation of small γ' -precipitates leads to a significant change in the stress–strain behavior, which can be mainly related to the change in chemical composition of the matrix and to the stress fields surrounding the precipitates [24, 35, 36]. TEM analyses conducted in these studies [36] revealed that aging in the martensite phase does not lead to the formation of small particles, which would affect phase transformation. It was concluded that changes in SC-SRO in Co–Ni–Ga alloys lead to a significant increase in transformation temperatures and eventually to a stabilization of the martensite [36]. In the current study, the stress hysteresis widths shown in Fig. 5 remain relatively constant between 25 and 50 MPa for both stress states and only slightly increase up to 200 °C. This is unusual since the critical stress for SIMT shows a relatively large temperature dependence, especially under compression (Fig. 4). Yet, the results are in good agreement with the evolution of permanent strain in this temperature range, as there is only a small accumulation of permanent strain below 200 °C. This further supports the conclusion that the matrix is hard enough to resist dislocation glide: both, the results of the cyclic stress–strain response (Figs. 1, 2) as well as the results of stress hysteresis obtained from single cycle experiments (Fig. 5) correlate well. For the cases shown in Figs. 1 to 3, diffusion is not negligible as the total dwell time in the cycling experiments was about 8.5 h. Thus, the formation of small γ' -particles and a change in SC-SRO may have significantly contributed to the change in the superelastic properties of Co–Ni–Ga alloys within stage 2.

The neutron diffraction experiments shed further light on the mechanism leading to functional degradation of Co–Ni–Ga HT-SMA. Figure 6 compares three-dimensional peak profiles of the as-grown austenite phase and of the axially strained austenite phase found in the sample fatigued at

300 °C for 1000 cycles. In addition, peak profiles of the martensite phase upon fatigue are shown. These profiles allow to evaluate defect densities in the bulk material. In Fig. 7 the TOF, x - and z -detector peak widths are plotted against the d value of their corresponding reflection. A clear trend becomes evident: in z -direction (parallel to load axis) the peak width of fatigued austenite is significantly increased compared with the as-grown austenite, whereas in x -direction (perpendicular to load axis) no significant peak broadening is observed. Note, that peak profiles of the as-grown austenite show slight elongation in z -direction. This effect is due to the neutron beam being scattered at each point of the sample causing a mapping of the elongated sample shape onto the detector. In some cases the error is quite high due to the fact that only a few symmetrically equivalent peaks were detected on equivalent backscattering detector pixels, which results in relatively large error bars on some reflections. The effect of peak broadening in z -direction is a superposition of an increase in dislocation density associated with an increase in single crystal mosaicity. Lattice strain accumulation can be well resolved by TOF peak broadening, which is caused by small deviations of the d value (Δd) from the mean value of a lattice plane. From Fig. 7a it can be deduced that fatigue leads to an increase of those deviations. This effect can be attributed to residual stresses between different domains as well as between the martensite and the strained austenite component in the sample [37]. In x -direction peak broadening of fatigued austenite cannot be resolved. In z -direction, however, the peak broadening is significant. This indicates a strong contribution from dislocations and mosaicity, clearly governed by the tensile cycling, since the z -direction is oriented parallel to the loading direction and parallel to the tetragonal axis of the martensite variant stabilized by uniaxial load. Figure 6 illustrates peak profiles of the as-grown and fatigued state, where a pronounced peak broadening can easily be observed in z -direction of the (hh0)-type slip planes and (350) planes indicating a slip plane independent increase in mosaicity. The comparison of the as-grown condition and the fatigued condition after 1000 cycles at 300 °C demonstrates that cyclic phase transformation is accompanied by intense formation of defects. Analysis of the diffraction intensities shows that the volume fractions of stabilized martensite and residual austenite are 94 ± 2 and 6 ± 2 %, respectively, after fatigue testing for 8.5 h at 300 °C. The small amount of residual austenite is probably interfaced with the martensite and thus is subjected to stresses leading to tetragonal strain. The results shown from the neutron diffraction experiments further emphasize the dominant role of dislocations on functional degradation in Co–Ni–Ga HT-SMA.

The spatial resolution of TEM analysis adds microstructural clues to the fatigue process. Figure 8 shows

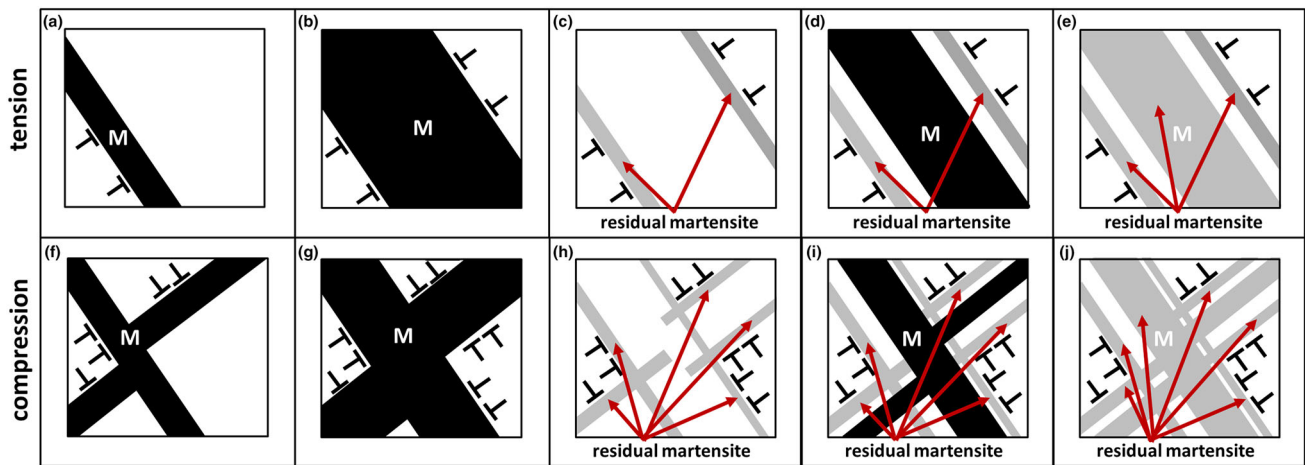


Fig. 9 Schematic illustrating the dislocation controlled stabilization of martensite for both stress states. **a, f** Initial loading, **b, g** maximum load, **c, h** unloaded, **d, i** subsequent re-loading and **e, j** final unload at 300 °C indicating the high volume fraction of stabilized martensite

the results of the TEM investigations of the sample fatigued for 1000 cycles at 300 °C. The selected area electron diffraction (SAED) pattern (Fig. 8c) clearly indicates that the sample is predominantly martensitic. In perfect agreement with the findings of neutron diffraction most of the sample is containing stabilized martensite. Due to the small area probed by TEM, the small volume fraction of residual austenite observed in the neutron diffraction analysis was not resolved in the SAED patterns. However, based on the TEM results, the proposed degradation mechanism, i.e., the dislocation-controlled pinning of martensite, can be validated. Martensite stabilization imposed by the SC-SRO mechanisms has been investigated in related work [36]. It was shown for Co–Ni–Ga that aging in martensite at elevated temperatures leads to stabilization of the product phase [36]. Similar processes could also be active in Co–Ni–Ga during cyclic loading. As a change in SC-SRO is fully reversible [36], martensite stabilization was fully reversible as well. Increase of temperature to a value above A_s of the Co–Ni–Ga alloy aged in martensite, i.e., to 400 °C, led to a re-ordering and, following a given dwell time, the loss of martensite stabilization [36]. In the current work, in situ heating in the TEM up to a temperature above 500 °C (not shown) did not result in a reverse transformation to austenite. Thus, martensite stabilization due to dislocation pinning seems to dominate cyclic degradation after long-term superelastic cycling. Furthermore, the pronounced dislocation activity is in line with the evolution of permanent strain (Fig. 3) and stress hysteresis (Fig. 5). Increased dislocation motion is accompanied by an evolution of residual macroscopic strain and an increased energy dissipation [7, 33]. Obviously, evolution of residual strain can result from a diffusion-controlled mechanism as well. Figure 8b, c, however, reveal that no precipitates were formed, at least in the fully

martensitic area probed, during superelastic cycling for 8.5 h. Niendorf et al. showed that finely dispersed particles formed after aging at 300 °C for 8.5 h in the austenitic phase [36]. Clearly, the impact of dwell time and mechanical deformation on microstructural evolution needs to be addressed in more detail in future work. However, by comparing the results of the present study and related work [36], it is evident, that static aging in the martensitic phase is different from aging in cyclically induced martensite. Picornell et al. [14] reported for Co–Ni–Ga that both phases, austenite and martensite, can be stabilized during heating, but it is not clear yet, if this “dual phase” stabilization is present during cyclic loading. Similarly, Niendorf et al. showed that different phase fractions can be stabilized simultaneously when applying aging in martensite at different degrees of macroscopic strain, i.e., different fractions of martensite and austenite [36]. The total dwell time (8.5 h) at elevated temperature was the same as in the current and in previous work [36]. It should be noted, however, that the effective dwell time for a given phase is less in the cyclic experiments. Still, the stress–strain response could be significantly affected by the formation of either precipitates or martensite stabilized through the SC-SRO mechanism. However, from the neutron diffraction experiments and the TEM results it appears that the dislocation-controlled stabilization of the martensite phase is the dominating mechanism. No direct evidence for the presence of precipitates or martensite stabilized through SC-SRO was found in the current study. Still, the slight increase in accumulated permanent strain at higher number of cycles (Fig. 3), which is similarly present for both stress states, cannot be solely explained by dislocation plasticity as absolute values of stresses are fundamentally different (Figs. 1, 2, 4). For trained Co–Ni–Ga single crystals Dadda et al. [22] revealed the presence of “ghost-like” martensite,

a clear indication for SC-SRO. Thus, it is probable that under the current loading conditions martensite is stabilized similarly cycle by cycle and subsequently pinned by dislocations. Obviously, the total dwell time for the first martensite band formed at 300 °C is higher than that for the martensite formed later during cycling. Repeated phase transformation events may introduce dislocations in the vicinity of already stabilized martensite, leading to mechanical pinning of primarily aging-stabilized martensite. This could be an explanation for the thermal stability of the stabilized martensite even upon heating above 500 °C.

Figure 9 illustrates the dislocation-controlled degradation mechanism inferred from the results obtained. Figure 9a, f shows the difference in martensite variant activity in the first cycle at a test temperature of 300 °C for both stress states. Due to the low matrix strength at 300 °C dislocations can form in each case. As a result of the multi-variant martensite transformation [22], more dislocations will be present in the compression case. Upon further loading (Fig. 9b, g) dislocation density increases during both, tension and compression loading. Thereby, a higher amount of permanent strain accumulates under compression due to intensive variant–variant interaction. Upon unloading a specific volume fraction of martensite is pinned within the austenite matrix (Fig. 9c, h) resulting in a decrease of the fraction of transformable matrix in the subsequent cycle (Fig. 9d, i). Following 1000 cycles into fatigue the major volume of the samples remains in martensitic condition mainly due to dislocation pinning (Fig. 9e, j).

Conclusions

The present study focused on martensitic transformation asymmetry during tensile and compressive loading of [001]-oriented $\text{Co}_{49}\text{Ni}_{21}\text{Ga}_{30}$ shape memory single crystals using superelastic cycling experiments, neutron diffraction analysis and microstructural characterization. The major findings can be summarized as follows:

1. A distinct tension–compression asymmetry in the superelastic stress–strain response was observed. The materials possess perfect cyclic stability up to 200 °C in tests that were run up to 1000 superelastic cycles. However, pronounced cyclic degradation sets in above 200 °C. The main underlying mechanism was identified as stabilization of martensite due to intense dislocation plasticity. In compression, martensite variant–variant interactions result in higher dislocation activity, and thus, more rapid functional degradation.
2. Below 100 °C, the stress hysteresis width was found to be similar for tension and compression. Above 100 °C, stress–strain hysteresis under compressive loads

increases more strongly with temperature than during tensile loading. This is attributed to the formation of multiple martensite variants under compression, leading to more pronounced defect generation and resulting in more internal friction at the phase boundaries.

3. Neutron diffraction analysis and TEM investigations revealed the presence of a high volume fraction of stabilized martensite. After 1000 superelastic cycles at 300 °C the pronounced dislocation plasticity seems to be the dominant degradation mechanism, which is promoted by the decreased strength of the matrix at this high temperature. Under the given loading conditions, diffusion-controlled degradation seems to be of minor importance.

Acknowledgments Financial support by the Deutsche Forschungsgemeinschaft (DFG) within the Research Unit Program “Hochtemperatur-Formgedächtnislegierungen” (Contract Nos. NI1327/3-1; MA1175/34-1; SCHM930/13-1 and EG101/22-1) is gratefully acknowledged.

References

1. Otsuka K, Wayman CM (1999) Shape memory materials. Cambridge University Press, Cambridge
2. Ma J, Karaman I, Noebe RD (2010) High temperature shape memory alloys. *Int Mater Rev* 55:257–315
3. Lagoudas D (2008) Shape memory alloys - modeling and engineering applications. Springer, New York
4. Morgan NB (2004) Medical shape memory alloy applications—the market and its products. *medical shape memory alloy applications—the market and its products. Mater Sci Eng A* 378:16–23
5. Sehitoglu H, Karaman I, Zhang XY, Chumlyakov Y, Maier HJ (2001) Competing mechanisms and modeling of deformation in austenitic stainless steel single crystals with and without nitrogen. *Scr Mater* 44:779–784
6. Kokorin VV, Samsonov YuI, Chernenko VA, Shevchenko OM (1989) Superelasticity in Fe-Ni-Co-Ti alloys. *Phys Met Metall* 67:202–204
7. Krooß P, Somsen C, Niendorf Schaper M, Karaman I, Chumlyakov Y, Eggeler G, Maier HJ (2014) Cyclic degradation mechanisms in aged FeNiCoAlTi shape memory single crystals. *Acta Mater* 79:126–137
8. Van Humbeeck J, Janssen J, Mwamba-Ngoie Delaey L (1984) The stabilisation of step-quenched copper-zinc-aluminum martensite part I: the reverse transformation temperatures. *Scr Metall* 18:893–898
9. Abu-Arab A, Chandrasekaran M, Ahlers M (1984) Martensite aging and its stabilization in Cu-Zn-Al shape memory alloys. *Scr Metall* 18:709–714
10. Otsuka K, Ren X (2001) Mechanism of martensite aging effects and new aspects. *Mater Sci Eng A* 312:207–218
11. Ren X, Otsuka K (1997) Origin of rubber-like behavior in metal alloys. *Nature* 389:579–582
12. Chernenko VA, Pons J, Cesari E, Zaslachuk IK (2004) Transformation behaviour and martensite stabilization in the ferromagnetic Co–Ni–Ga Heusler alloy. *Scr Mater* 50:225–229
13. Kustov S, Pons J, Cesari E, Van Humbeeck J (2004) Pinning-induced stabilization of martensite Part I. Stabilization due to static pinning of interfaces. *Acta Mater* 52:3083–3096

14. Picornell C, Pons J, Cesari E, Chumlyakov YI, Dutkiewicz J (2009) Effect of aging under compressive stress along [100] in Co-Ni-Ga single crystals. *Funct Mater Lett* 2:83–86
15. Buenconsejo PJS, Kim HY, Hosoda H, Miyazaki S (2009) Shape memory behavior of Ti-Ta and its potential as a high-temperature shape memory alloy. *Acta Mater* 57:1068–1077
16. Buenconsejo PJS, Kim HY, Miyazaki S (2009) Effect of ternary alloying elements on the shape memory behavior of Ti-Ta alloys. *Acta Mater* 57:2509–2515
17. Atli KC, Karaman I, Noebe RD (2011) Work output of the two-way shape memory effect in Ti_{50.5}Ni_{24.5}Pd₂₅ high-temperature shape memory alloy. *Scr Mater* 65:903–906
18. Karaca HE, Acar E, Ded GS, Saghaian SM, Basaran B, Tobe H, Kok M, Maier HJ, Noebe RD, Chumlyakov YI (2015) Microstructure and transformation related behaviors of a Ni_{45.3}Ti_{29.7}Hf₂₀Cu₅ high temperature shape memory alloy. *Mater Sci Eng A* 627:82–94
19. Mohanchandra KP, Shin D, Carman GP (2005) Deposition and characterization of Ti-Ni-Pd and Ti-Ni-Pt shape memory alloy thin films. *Smart Mater Struct* 14:312–316
20. Firstov GS, Van Humbeeck J, Koval YN (2004) High-temperature shape memory alloys: some recent developments. *Mater Sci Eng A* 378:2–10
21. Dadda J, Maier HJ, Karaman I, Karaca HE, Chumlyakov YI (2006) Pseudoelasticity at elevated temperatures in [001] oriented Co₄₉Ni₂₁Ga₃₀ single crystals under compression. *Scr Mater* 55:663–666
22. Dadda J, Maier HJ, Karaman I, Karaca HE, Chumlyakov YI (2010) Tension - compression asymmetry in Co₄₉Ni₂₁Ga₃₀ high-temperature shape memory alloy single crystals. *Int J Mater Res* 101:1503–1513
23. Niendorf T, Dadda J, Lackmann J, Monroe JA, Karaman I, Panchenko E, Karaca HE, Maier HJ (2013) Tension - compression asymmetry in Co₄₉Ni₂₁Ga₃₀ high-temperature shape memory alloy single crystals. *Mater Sci For* 82:738–739
24. Kireeva IV, Picornell C, Pons J, Kretinina IV, Chumlyakov YI, Cesari E (2014) Effect of oriented γ precipitates on shape memory effect and superelasticity in Co-Ni-Ga single crystals. *Acta Mater* 68:127–139
25. Kireeva IV, Pons J, Picornell C, Chumlyakov YI, Cesari E, Kretinina IV (2013) Influence of γ nanometric particles on martensitic transformation and twinning structure of L1₀ martensite in CoNiGa ferromagnetic shape memory single crystals. *Intermetallics* 35:60–66
26. Monroe JA, Karaman I, Karaca HE, Chumlyakov YI, Maier HJ (2010) High-temperature superelasticity and competing microstructural mechanisms in Co₄₉Ni₂₁Ga₃₀ shape memory alloy single crystals under tension. *Scr Mater* 62:368–371
27. Li Y, Xin Y, Chai L, Ma Y, Huibin X (2010) Microstructures and shape memory characteristics of dual-phase Co-Ni-Ga high-temperature shape memory alloys. *Acta Mater* 58:3655–3663
28. Dogan E, Karaman I, Chumlyakov YI, Lou ZP (2011) Microstructure and martensitic transformation characteristics of CoNiGa high temperature shape memory alloys. *Acta Mater* 59:1168–1183
29. Dadda J, Maier HJ, Niklasch D, Karaman I, Karaca HE, Chumlyakov YI (2008) Pseudoelasticity and cyclic stability in Co₄₉Ni₂₁Ga₃₀ shape-memory alloy single crystals at ambient temperature. *Mater Trans A* 39:2026–2039
30. Sehitoglu H, Hamilton R, Canadinc D, Zhang XY, Gall K, Karaman I, Chumlyakov Y, Maier HJ (2003) Detwinning in NiTi alloys. *Mater Trans A* 34:5–13
31. Keen DA, Gutmann MJ, Wilson CC (2006) SXD - the single-crystal diffractometer at the ISIS spallation neutron source. *J Appl Cryst* 39:714
32. Gall K, Maier HJ (2002) Cyclic deformation mechanisms in precipitated NiTi shape memory alloys. *Acta Mater* 50:4643–4657
33. Simon T, Kroeger A, Somsen C, Dlouhy A, Eggeler G (2010) On the multiplication of dislocations during martensitic transformations in NiTi shape memory alloys. *Acta Mater* 58:1850–1860
34. Dadda J, Canadinc D, Maier HJ, Karaman I, Karaca HE, Chumlyakov YI (2007) Stress-strain-temperature behaviour of [001] single crystals of Co₄₉Ni₂₁Ga₃₀ ferromagnetic shape memory alloy under compression. *Phil Mag* 87:2313–2322
35. Chumlyakov YI, Kireeva IV, Panchenko EY, Kirillov VA, Timofeeva EE, Kretinina IV, Daniilov YN, Karaman I, Maier HJ, Cesari E (2012) Thermoelastic martensitic transformation in single crystals with disperse particles. *Russ Phys J* 54:937–950
36. Niendorf T, Krooß P, Chumlyakov YI, Maier HJ (2014) Martensite aging - an avenue to new high temperature shape memory alloys. *Acta Mater* 89:298–304
37. Kužel R (2007) Kinematical diffraction by distorted crystals—dislocation X-ray line broadening. *Z Kristallogr* 222:136–149